









Pioneering High-Speed Pulsar Parameter Estimation Using Convolutional Neural Networks

Greg Olmschenk ^{1,2} Emily Broadbent ^{1,3,4,5} Constantinos Kalapotharakos ¹ Wendy F. Wallace ^{1,3,4}
Thibault Lechien ^{1,3,4,6} Zorawar Wadiasingh ¹ Demosthenes Kazanas ^{1,2} and Alice Harding ⁷

¹*NASA Goddard Space Flight Center, Greenbelt, MD 20771, USA*

²*Department of Astronomy, University of Maryland, College Park, MD 20742, USA*

³*Center for Research and Exploration in Space Science and Technology, NASA/GSFC, Greenbelt, MD 20771, USA*

⁴*Southeastern Universities Research Association, Washington, DC 20005 USA*

⁵*Department of Astronomy and Astrophysics, University of California San Diego, La Jolla, CA 92093, USA*

⁶*Max Planck Institute for Astrophysics, Karl-Schwarzschild-Straße 1, 85748 Garching bei München, Germany*

⁷*Theoretical Division, Los Alamos National Laboratory, Los Alamos, NM 87545, USA*

Accurate thermal emission models of neutron stars are essential for constraining the dense matter equation of state. However, incorporating realistic magnetic field structures is computationally prohibitive, severely constraining feasible parameter space exploration. In this work, we develop a neural network (NN) emulator to generate model thermal bolometric X-ray light curves of millisecond pulsars with multipolar magnetic fields. We assess the NN's predictive and computational performance across a broad parameter space. We find that for a static vacuum field (SVF) model, the NN provides a >400 times speedup. We integrate this NN emulator into a Monte Carlo Markov Chain (MCMC) framework to replace the computationally expensive physical model during parameter exploration. Applied to PSR J0030+0451, this approach allows the MCMC to reach equilibrium in ~ 1 day on 4000 cores, where with the original physical model alone it would have taken more than a year on the same hardware. We compare posterior distributions by running equivalent MCMC iterations with both the NN and the physical model, evaluate differences in distributions when continuing the physical model MCMC from the NN MCMC equilibrium state, and assess variations in posterior distributions resulting from NNs trained on datasets of different sizes. Our NN architecture is agnostic to the underlying physics of the physical model and can be trained for any other physical model, opening many avenues of analysis that were previously intractable. The NN speed remains the same regardless of the complexity of the physical model it was trained to emulate, allowing even greater speedups for physical models that are more complex than the SVF model.

INTRODUCTION

Understanding neutron stars (NSs) and their equation of state (EoS) has important implications for cold dense matter and fundamental physics. The millisecond pulsar PSR J0030+0451 [1, 2] has provided strong evidence for multipolar magnetic fields through modeling of its X-ray phase-folded light curve (LC) [3–5]. These X-rays arise from deep heating by bombardment from charges at magnetic polar caps; PSR J0030+0451 exhibits a distinctly asymmetric LC demanding departures from a centered dipole field. To constrain the underlying multipolar magnetic field structure of PSR J0030+0451, [6] investigated magnetic field structures that comprised offset dipole-plus-quadrupole components using SVF and force-free global magnetosphere models, uncovering several degenerate parameter solutions for bolometric LCs. However, deriving detailed MCMC posterior parameter distributions of these models is prohibitively computationally expensive. In this work, we develop a NN surrogate model that replaces the physical models during MCMC parameter exploration, achieving an unprecedented speedup while preserving accuracy and enabling a comprehensive exploration of parameter space previously not possible. This also sets the stage for future surrogate models that incorporate additional physics and parameters required to advance

beyond bolometric LCs.

PHYSICAL MODEL

The methods used in this work for the SVF as well as the MCMC implementation, are those used in Kalapotharakos *et al.* [6].

Briefly, the method employs a ray-tracing approach utilizing the Kerr metric that integrates photon trajectories from a distant observer image plane to the stellar surface hot spots, with Doppler boosting [e.g., 7]. The model assumes that emission originates from hot spots coinciding with the polar caps, *i.e.*, the regions on the stellar surface corresponding to the origin of open¹ magnetic field lines.

For the dipole component, the parameters are the 3 Cartesian offset position coordinates relative to the NS center $\{x_D, y_D, z_D\}$, the inclination angle α_D , and the azimuthal direction of its moment ϕ_D . For the quadrupole component, the parameters are the 3 Cartesian offset position coordinates $\{x_Q, y_Q, z_Q\}$, the inclination angle α_Q , and the azimuthal direction of its moment ϕ_Q . An addi-

¹ Open field lines are considered those that cross the light cylinder.

tional parameter is the relative strength of the quadrupole moment B_Q/B_D at a distance equal to the NS radius.

Throughout the remainder of this work, unless otherwise specified, the “physical model” refers to the SVF bolometric thermal X-ray LC model. Additionally, in this study, we utilize the photon library, simplified atmosphere model, and LC normalization from Kalapotharakos *et al.* [6], with the stellar mass, radius, and observer angle fixed to the highest loglikelihood values provided by Riley *et al.* [4].

SIMULATED DATASET

The simulated dataset consists of parameter sets and the corresponding model X-ray LCs produced using the SVF model described in Physical Model Section. The dataset used to train and evaluate the NN model is generated in two steps.

First, LCs are generated for approximately 8×10^6 random parameter sets uniformly distributed across the entirety of reasonable parameter space. However, an additional constraint ensures that the offsets of the dipole and quadrupole moments do not exceed 0.7 of the stellar radius.

Second, for each parameter set, 63 additional cases are generated by considering a full 360° rotation in 64 steps, corresponding to the 64 phase bins of the bolometric NICER X-ray LCs. This is achieved by rotating the offsets and magnetic moment orientations and applying a corresponding shift to the LC. This approach takes advantage of rotational symmetry to augment the dataset by a factor of 64 without recalculating the physical model LCs.

The total size of the simulated dataset is approximately $8 \times 64 \times 10^6 \approx 5 \times 10^8$ samples. From this dataset, 10^5 samples are used for validation and another 10^5 samples for testing. The remainder is used for training. When splitting the dataset, no rotation-augmented versions of a LC from the training dataset were included in the validation or test dataset, and vice versa. Except for grouping rotation augmented LCs in the same split of the data, splitting between training, validation, and testing is random. It is worth noting that, in the context of an 11-dimensional parameter space, 5×10^8 data points still represent a relatively sparse sampling (*i.e.*, ≈ 6 points per dimension for a uniform grid).

The validation dataset is used to monitor the performance of the network on unseen data throughout the training process, while the test dataset is reserved for final evaluation to assess the NN’s ability to generalize to unseen data.

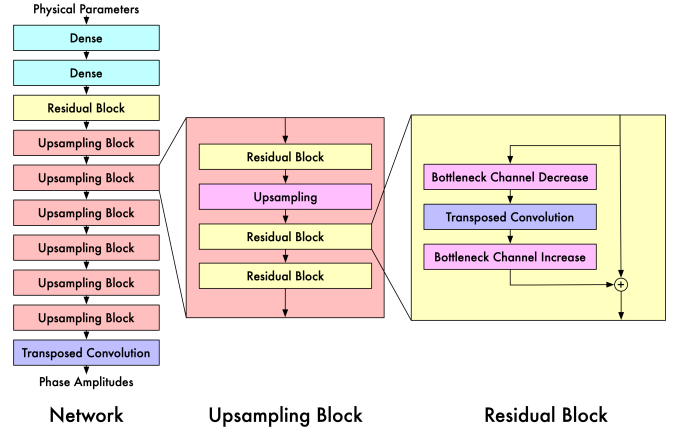


Figure 1. An overview diagram of the neural network model used in this work. The network is a ResNet-like model, except 1D and transposed.

NEURAL NETWORK PIPELINE

Figure 1 shows an overview diagram of the NN model used in this work. The network is a ResNet-like model [8], except 1D and transposed. The network contains 60 trainable layers and $\sim 2 \times 10^7$ trainable parameters.

Briefly, in addition to the standard advantages of a convolutional neural network (CNN, 9) (*e.g.*, weight sharing), a CNN is apt for this task as feature locality is important in phase-folded LCs, and these networks explicitly take this into account. ResNet architectures are robust structures that have been thoroughly tested on an enormous number of tasks. The specific architecture we built for this task was designed based on prior experience working with other LC applications. Notably, the architecture includes no structure or mechanisms explicitly designed for SVF modeling and can be trained to emulate other physical models. Our full NN code, including all network architecture details, is open-source and available at <https://github.com/golmschenk/haplo>.

Training time

While the trained NN’s LC generation is orders of magnitude faster than the physical model’s, it is important to note that there is an upfront training time cost before the NN can be used for this purpose. During our various experiments, the longest total training time a NN received was ~ 15 days when being trained across 128 Nvidia A100 GPUs on NASA’s *Pleiades*. While this training cost is not insignificant, as we will see in Evaluation Section, the computational cost is much lower than running a single MCMC of the physical model to convergence. Furthermore, the model only needs to be trained once, and then can be used for any number of viable solutions (such as the degenerate solutions presented in Kalapotharakos

et al. 6). Future models that include stellar mass, radius, and period parameters will additionally be able to be used for any number of NSs. From this point of view, the upfront training cost approaches comparative insignificance. Reasonable results can also be obtained with far less training time than that given above. For example, when training with our smaller 5M dataset, we reach training convergence in about 1 day, and, as will be seen in Figure 1, the model trained in this way produces a similar posterior distribution for the observed data. Subsequent training times may also be reduced by fine-tuning from existing trained models rather than from random initial conditions.

EVALUATION

Light curve reconstruction accuracy on simulated data

To compare the NN’s reconstruction performance, we compare the NN predicted LC against the LC generated by the physical model using the following median normalized squared error (MdNSE) metric,

$$\text{MdNSE} = \frac{\sum_i (y_i - \hat{y}_i)^2}{\text{median}(\hat{y})^2}, \quad (1)$$

where y is the predicted LC and \hat{y} is the physical model LC. The MdNSE was chosen as a stand-in for χ^2 for multiple reasons. First, the simulated data does not have associated error values, which are essential for the computation of χ^2 . Even assuming Poissonian noise for χ^2 calculations is non-trivial, as it depends on the number of photon detections and the assumed distance to the NS, introducing complexities that are difficult to standardize. Furthermore, the LCs have amplitudes that vary by orders or magnitude. Using χ^2 would treat higher-amplitude LCs as inherently more important, leading to evaluation biases. In contrast, the MdNSE metric, by normalizing using the median of the physical model LC, treats all LCs more or less equally, focusing on their shape rather than amplitude. The NN is trained to minimize the $\log_{10}(\text{MdNSE})$.

Figure 2 presents a representative comparison of LCs produced by the physical model and the best-performing NN model. For an impartial sampling, the LCs shown are those at various quantile thresholds of fitting performance. Even the phase-folded LC corresponding to the 97.75th percentile of MdNSE shows reasonable agreement with the physical model upon visual inspection. However, it is important to note that a good fit in terms of MdNSE does not always correspond to a visually good fit. For example, cases where the difference between the maximum and minimum values of the LC is much smaller than its median value can result in discrepancies that are less visually intuitive.

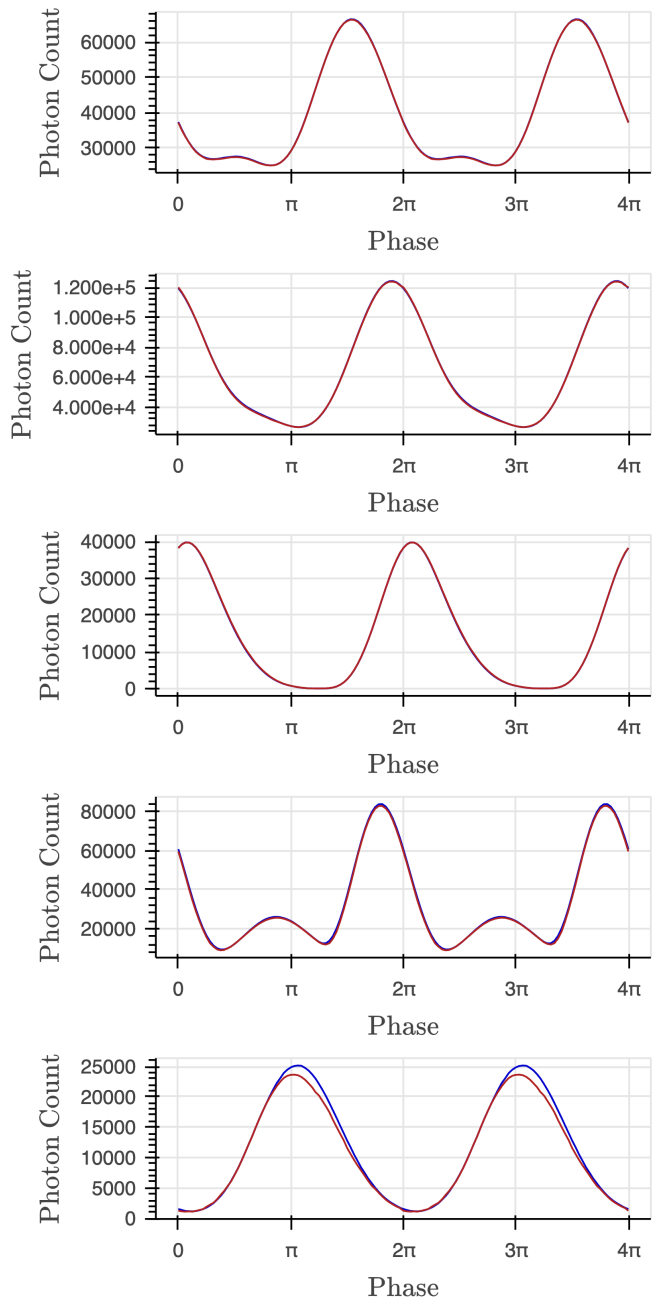


Figure 2. A comparison of light curves produced from the physical model (blue) and the best neural network model (red). From top to bottom, the cases shown are those at quantile 0.0225, 0.159, 0.5, 0.841, and 0.9775 of fits sorted by MdNSE.

Figure 3 shows the distributions of MdNSE values in log space when reconstructing LCs from the random test dataset using NNs trained on varying dataset sizes, ranging from 500k to 500M samples. All distributions exhibit a Gaussian distribution shape in $\log(\text{MdNSE})$, with both the mean and median values shifting to lower MdNSE values and the standard deviation decreasing as the training dataset size increases. This trend indicates improved re-

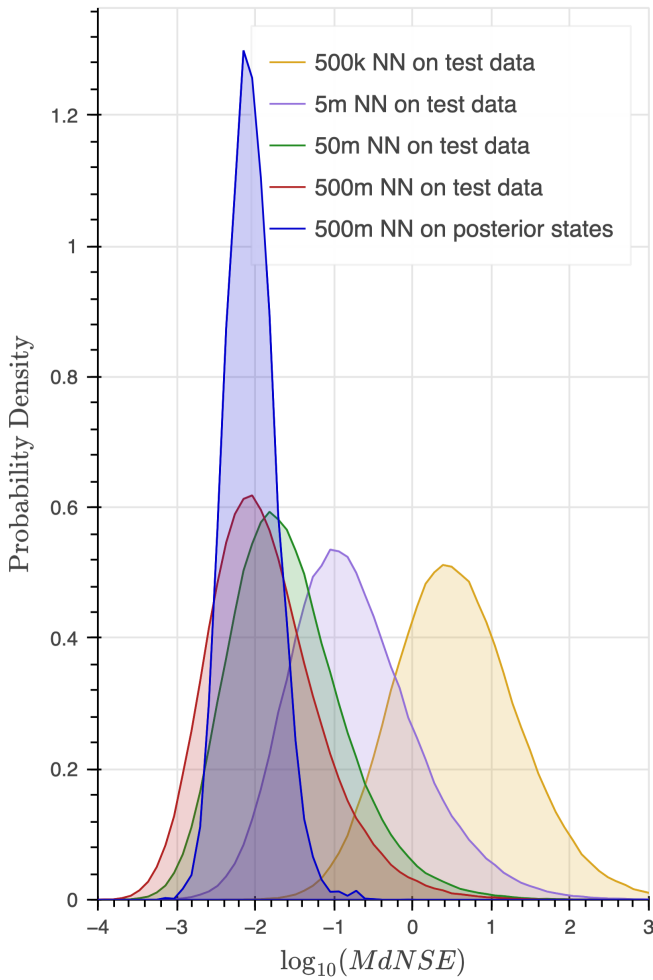


Figure 3. A comparison of the MdNSE distributions of light curve reconstruction on the test dataset and for simulated data using parameter states from an MCMC for PSR J0030+0451. Distributions are shown for the MdNSE values for neural networks trained with 500M (red), 50M (green), 5M (purple), and 500K (yellow) samples when applied to the test dataset, with the network progressively improving with more training data. The blue distribution shows the MdNSE distribution of the best NN (trained with 500M samples) when applied to the parameter states from an MCMC for PSR J0030+0451 run using the physical model.

construction accuracy with larger training datasets. The best performing NN model is the one trained with 500M samples. Unless otherwise specified, any reference to the NN model is referring to this version of the trained network.

Distribution reconstruction accuracy on real data

Figure 4 shows a comparison of the posterior distributions for PSR J0030+0451 as estimated via MCMC runs using the physical model to produce LCs (blue) and the NN model (red). Both MCMC runs started from

the same initial conditions as the MCMC run that produced the RV1 solution presented in Kalapotharakos *et al.* [6] and were executed with approximately 8192 parallel chains, all iterated for 8000 steps, more than twice the number of steps used in Kalapotharakos *et al.* [6]. The physical model MCMC run required 5 days on 4000 Intel Broadwell cores, making further evolution computationally prohibitive. By comparison, on the same hardware, the NN model MCMC run completed the same number of iterations in a small fraction of the time, i.e., ~15 minutes.

In the table shown within the figure, for the 1D marginalized distributions, the credible interval required to encompass the median value of the distribution from the other method is shown (CI for median). As there are two distributions that contain CIs for the other distribution’s median to fall within, the larger of these two values is the one that is given here. From this, we see the median of one distribution is always well within the 68.27% credible interval (1σ) of the other, and is below 15% in most cases. This provides an initial intuitive indication of the NN’s reliability in replicating the posterior results of the physical model.

To more thoroughly quantify the similarity between the distributions, we compute the Wasserstein distance (WD, 10), a metric that evaluates the difference between two probability distributions, capturing details beyond the median and standard deviation. The parameter values are first normalized using their modified Z -scores, ensuring standardization across the distributions. The mean WD is then calculated for the normalized 1D marginal distributions, providing a robust measure of the discrepancy between the NN and physical model results. We also include the Jensen–Shannon divergence (JSD, 11) and Kolmogorov–Smirnov statistic (KS, 12) values. However, they show similar trends to WD. For all three metrics, a value of zero would show perfect agreement.

The distribution comparison metrics for each parameter are displayed within the corner plot, offering a direct visual comparison between the posterior distributions and their quantified differences. The results demonstrate that the NN model closely agrees with the physical model, even for higher-dimensional parameter spaces. Importantly, the spread of the NN-based posterior distributions is consistent with the physical model, suggesting that the NN faithfully reproduces not only the central tendencies but also the variability of the underlying parameter space.

In Figure 3, we also show the $\log(\text{MdNSE})$ distribution of the LCs corresponding to the above posterior distribution. Although this $\log(\text{MdNSE})$ distribution is narrower than the corresponding distribution for the 500M NN on all of reasonable parameter space, the two distributions are comparable around the same median value. This suggests that the NN’s performance in reproducing the posterior distribution of PSR J0030+0451 is not an outlier and similar performance can be expected for other regions of parameter space.

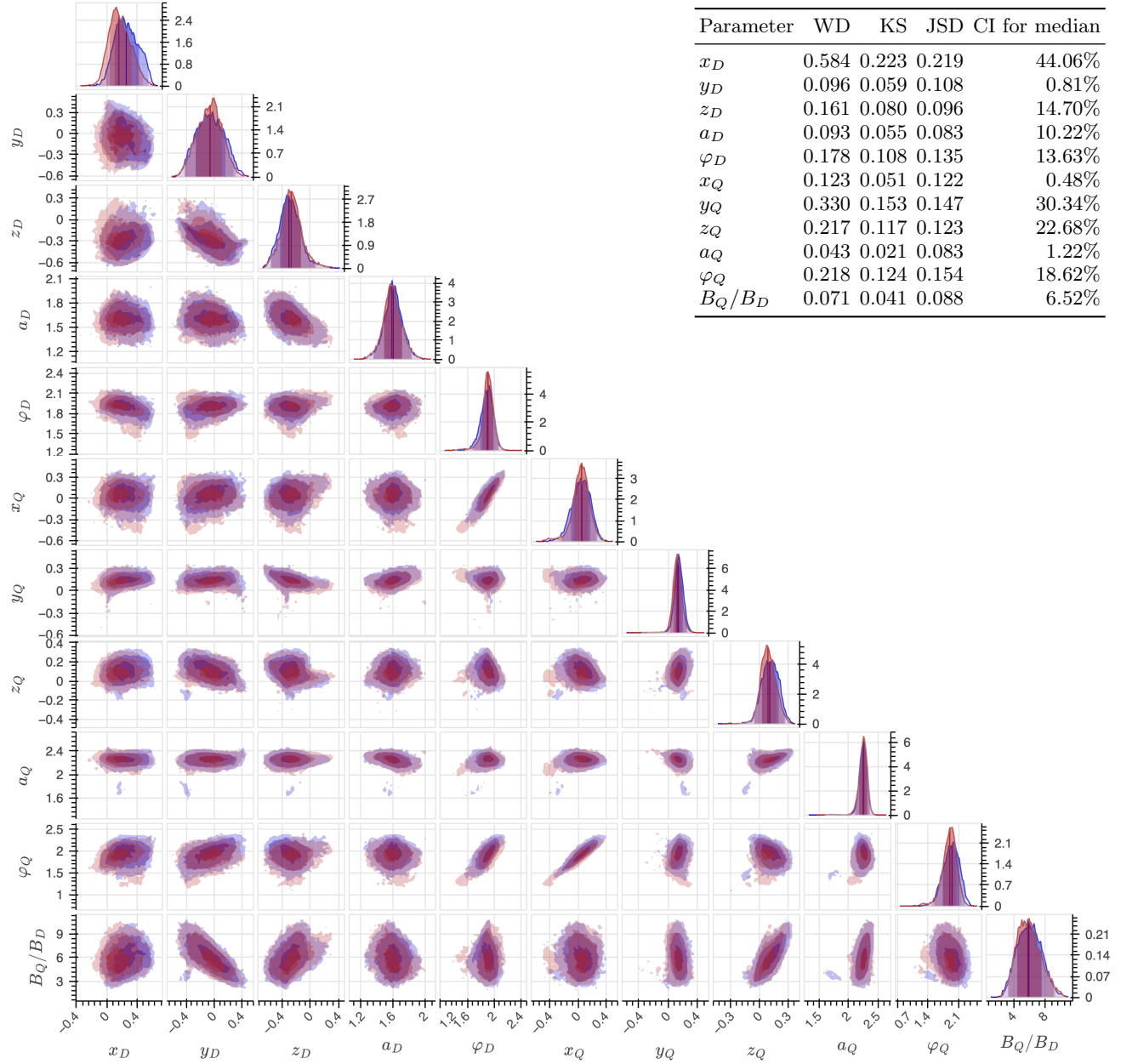


Figure 4. A comparison of the PSR J0030+0451 posterior distributions from the MCMC with light curves generated by the physical model (blue) and the best neural network model (red). Both MCMCs executed approximately 8192 parallel chains for 8000 steps. The physical model version took ~ 5 days on 4000 cores. The neural network version took ~ 15 minutes on the same hardware. Metrics comparing the 1D marginal distributions between the posteriors is shown at the top right. Shown are the Wasserstein distance (WD), the Jensen–Shannon divergence (JSD), and the Kolmogorov–Smirnov statistic (KS). Also shown is the maximum credible interval required to encompass the median of the other distribution (CI for median).

With the computational speed achieved by the NN implementation, we were able to extend the MCMC explorations to approximately 1.5×10^6 iterations for the same 8192 parallel chains. This longer run converged to a posterior distribution that differed from the one derived from the shorter MCMC runs limited by the speed of

the physical model. Importantly, this longer run MCMC resulted in a posterior distribution that stabilized and remained consistent over the last 1 million iterations, providing strong evidence of convergence. Notably, this result, and a subsequent analysis of the physical model MCMC evolution, revealed that the solutions identified

in Kalapotharakos *et al.* [6] were not yet converged.

However, due to the computational expense of the physical model, evolving it for an equivalent number of iterations is infeasible, preventing direct comparison of these posterior distributions. To address this limitation, first, we performed a continuation study. Starting from the equilibrium posterior distribution of the 500M NN, we evolved the MCMC for an additional 4000 iterations using the physical model. The resulting posterior showed no significant variation from the converged NN-derived posterior, providing strong evidence that the NN-derived posterior accurately represents the distribution that the physical model would converge to with further exploration. A comparison of these two posterior distributions is shown in Figure 5. As a second verification, the posterior distribution generated by the NN trained with 5M samples was compared to those from the NN trained on the full 500M dataset. This comparison is shown in Figure 6. The agreement between these distributions indicates that the NNs achieve sufficient accuracy to enable reliable posterior estimation, even with reduced training data. The NN trained with 5M samples results in a different level of LC reconstruction accuracy (as shown in Figure 3) and exhibits only weak correlation with the NN trained with 500M samples. Yet, the fact that it still produces approximately the same converged posterior distribution as the 500M NN model provides additional evidence that NN-based MCMCs effectively reveal the true underlying posteriors. The NN trained with 50M samples shows comparable agreement.

This analysis highlights the effectiveness of the NN model as a computationally efficient surrogate for the physical model. By significantly reducing computational costs, the NN enables longer MCMC evolution and more thorough exploration of parameter space. Furthermore, the agreement between posterior distributions derived from the physical model, the best NN model, and NN models trained using smaller data subsets provides robust evidence of the NN’s accuracy and reliability.

DISCUSSION AND CONCLUSION

This work establishes NNs as a transformative tool for NS parameter inference, overcoming previous computational bottlenecks and enabling extensive parameter space exploration that was previously infeasible. By replacing computationally expensive physical models with a NN emulator, we achieve a speedup of over 400 times for SVF models, reducing MCMC run-times from days to minutes and from years to days. As the SVF models on bolometric LCs themselves are already simplified, this framework bodes favorably for surrogates of more advanced physical models that consider the full parameter space, including mass and radius. The NN’s speed enables previously unattainable parameter space exploration and evaluation

of posterior distribution convergence, overcoming prior computational limits.

One of the most significant outcomes of this work is the ability to achieve convergence in MCMC explorations, which was infeasible with the SVF physical model in Kalapotharakos *et al.* [6]. Extending the MCMC iterations to approximately 1.5 million with the NN, we find that the posterior distributions differ from those obtained in previously reported shorter MCMC runs. Importantly, the posterior stabilized and remained consistent for the final 1 million iterations, providing strong evidence of convergence. Direct comparisons with the physical model for such extended runs remain intractable due to their computational expense. However, validation experiments, including the physical model MCMC continuation from the NN-derived equilibrium state and NNs trained on considerably smaller datasets, indicate that the NN-derived posterior is an accurate representation of the underlying distribution.

The implications of these advancements are even more drastic for force-free (FF) magnetohydrodynamic field models of the global magnetosphere, where the physical model computations are at least three orders of magnitude slower than the SVF case for the same field parameters. Inference using the NN for FF LCs incurs no additional computational overhead, as the NN speed depends solely on its architecture. Our architecture has no structures or mechanisms explicitly geared toward any particular physical model, and the same network can be trained to emulate other modeling approaches. Preliminary results for the FF emulation show unprecedented speedups exceeding 10^6 times, bringing previously inaccessible analyses to practical time scales. These approaches are under active investigation and will be presented in Lechien *et al.* [13], where we expand the parameter space to include stellar mass, radius, and observer angle, further enhancing the scope of this framework.

Beyond computational speed, our extended exploration of the parameter space using the NN-accelerated approach unified certain solutions, such as RV1 and RV2 in Kalapotharakos *et al.* [6], which were initially thought to be distinct. However, other solutions, such as RV3 and RV4, remained distinct, suggesting the existence of multiple local log-likelihood maxima that are relatively prominent, suggesting significant competing regions within the parameter space. These results emphasize the importance of extensive MCMC sampling to explore the entire parameter space thoroughly, a current significant limitation in NICER analyses of millisecond pulsars. While all corresponding reduced χ^2 values remain well below 1, incorporating additional observational constraints, such as gamma-ray LCs, is crucial to refining the analysis and identifying dominant solutions, as previously demonstrated in Kalapotharakos *et al.* [6]. A comprehensive study along this direction is also going to be presented in Lechien *et al.* [13].

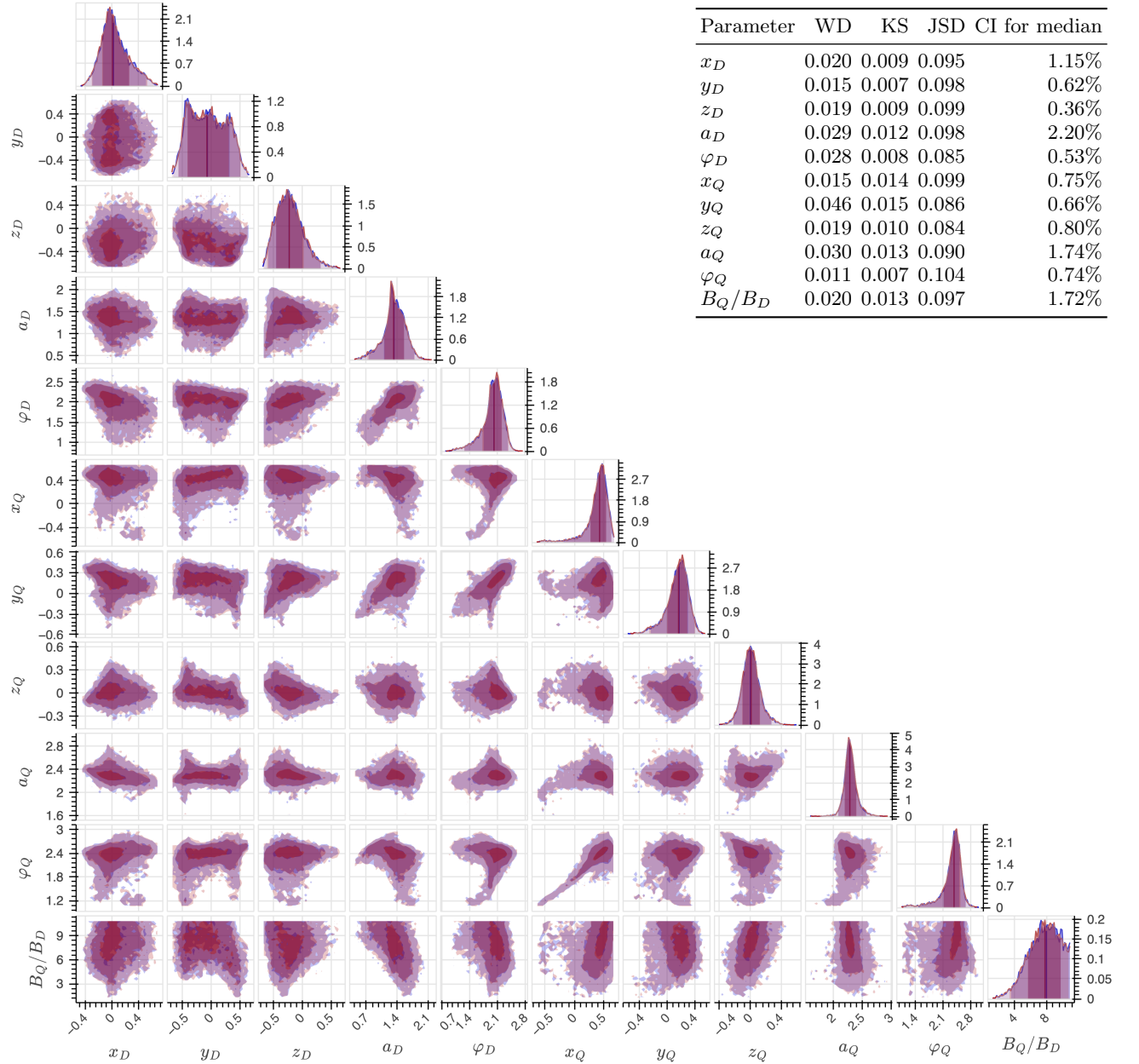


Figure 5. A comparison of the PSR J0030+0451 posterior distributions from the MCMC with light curves generated by the physical model (blue) and the best neural network model (red). In this case, the MCMC was run to convergence using the neural network model. Then, the physical model MCMC was continued from that converged state to investigate if it would diverge from the converged state found by the neural network MCMC. Using the neural network, the MCMC took approximately 1 day on 4000 cores to reach convergence. To reach the same number of MCMC iterations (and presumably the same convergence) using the physical model would take more than a year on the same hardware.

The NN architecture created for this work was chosen primarily based on prior experience in works with similar data structures. A more detailed investigation and experimental exploration of NN architectures is likely to produce superior models. We plan to carry out such exploration in future work. Additionally, several other technical avenues for improvement are available. For example, during the

MCMC run, we currently perform the LC inference using the NN on CPUs. Significant speed benefits are expected by using batched inference on GPUs.

In conclusion, this study establishes the NN emulator as a powerful and scalable surrogate for computationally expensive physical models in NS parameter inference. The demonstrated speedup not only enhances the feasi-

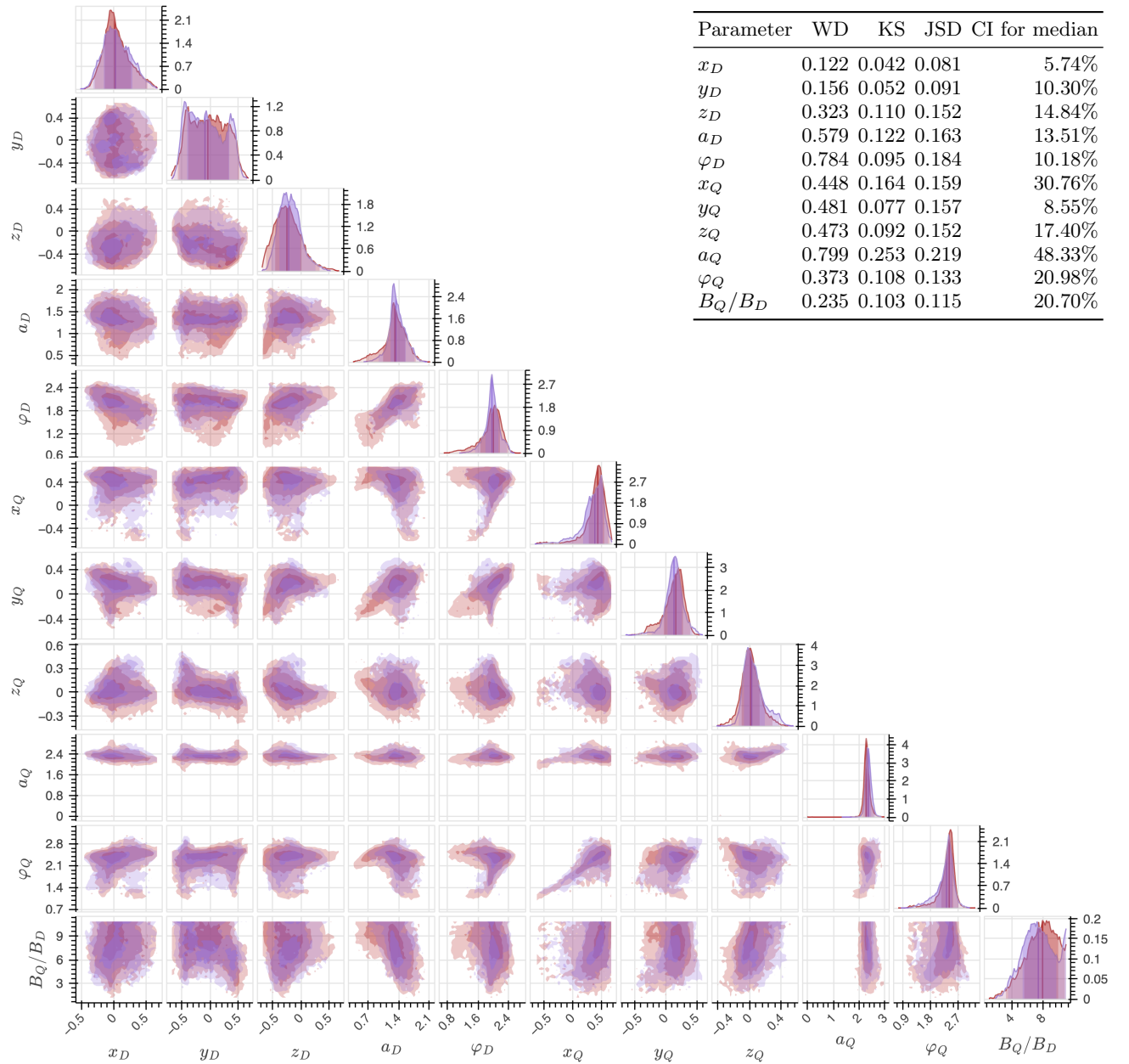


Figure 6. A comparison of the PSR J0030+0451 posterior distributions from the MCMC run to convergence with light curves generated by neural networks with differing amounts of training data. The networks were trained with 500M (red) and 5M (purple) training samples.

bility of MCMC-based analyses for SVF models but also paves the way for applications such as FF or other physical models, where computational gains are even more immense. By enabling extensive parameter space explorations and achieving robust convergence, this approach provides a more comprehensive understanding of NS properties. These innovations significantly advance efforts to constrain the dense matter equation of state, opening new avenues of research in the field and positioning NNs as

an indispensable tool for the future of NS analysis.

ACKNOWLEDGMENTS

The material is based upon work supported by NASA under award numbers 80GSFC21M0002, 80GSFC24M0006, 80NSSC21K1999, 22-ADAP22-0142, 22-TCAN22-0027, 21-ATP21-0116, and 22-FERMI22-

0035.

-
- [1] A. Somer, in *International Astronomical Union Colloquium*, Vol. 177 (Cambridge University Press, 2000) pp. 17–20.
- [2] N. D’Amico, in *International Astronomical Union Colloquium*, Vol. 177 (Cambridge University Press, 2000) pp. 27–30.
- [3] M. Miller, F. K. Lamb, A. Dittmann, S. Bogdanov, Z. Arzoumanian, K. C. Gendreau, S. Guillot, A. Harding, W. Ho, J. Lattimer, *et al.*, *The Astrophysical Journal Letters* **887**, L24 (2019).
- [4] T. E. Riley, A. L. Watts, S. Bogdanov, P. S. Ray, R. M. Ludlam, S. Guillot, Z. Arzoumanian, C. L. Baker, A. V. Bilous, D. Chakrabarty, *et al.*, *The Astrophysical Journal Letters* **887**, L21 (2019).
- [5] A. V. Bilous, A. L. Watts, A. K. Harding, T. E. Riley, Z. Arzoumanian, S. Bogdanov, K. C. Gendreau, P. S. Ray, S. Guillot, W. C. G. Ho, and D. Chakrabarty, *The Astrophysical Journal, Letters* **887**, L23 (2019), arXiv:1912.05704 [astro-ph.HE].
- [6] C. Kalapotharakos, Z. Wadiasingh, A. K. Harding, and D. Kazanas, *The Astrophysical Journal* **907**, 63 (2021).
- [7] D. Psaltis and F. Özel, *The Astrophysical Journal* **792**, 87 (2014), arXiv:1305.6615 [astro-ph.HE].
- [8] K. He, X. Zhang, S. Ren, and J. Sun, in *Proceedings of the IEEE Conference on Computer Vision and Pattern Recognition* (2016) pp. 770–778.
- [9] A. Krizhevsky, I. Sutskever, and G. E. Hinton, in *Advances in neural information processing systems* (2012) pp. 1097–1105.
- [10] V. M. Panaretos and Y. Zemel, *Annual review of statistics and its application* **6**, 405 (2019).
- [11] M. L. Menéndez, J. Pardo, L. Pardo, and M. Pardo, *Journal of the Franklin Institute* **334**, 307 (1997).
- [12] F. J. Massey Jr, *Journal of the American statistical Association* **46**, 68 (1951).
- [13] T. Lechien, C. Kalapotharakos, Z. Wadiasingh, G. Olmschenk, E. Broadbent, and D. Kazanas, “Multi-wavelength light curve neutron star parameter inference using neural networks,” (2025, in preparation), in preparation.